AIAA JOURNAL
Vol. 42, No. 9, September 2004

Noise Prediction of a Rectangular Jet Using Large-Eddy Simulation

B. Rembold[*] and L. Kleiser[†]
Swiss Federal Institute of Technology, CH-8092 Zurich, Switzerland

We investigate the acoustic radiation from a 1:5 aspect ratio transitional rectangular jet predicted by large-eddy simulation (LES). The approximate deconvolution model was used as subgrid-scale model. It was found in a previous study that the acoustic far-field prediction when Lighthill's analogy is applied to data from direct numerical simulation and LES agrees well for the low-frequency range. However, higher frequencies in the LES prediction have been contaminated by spurious noise. In the present study, the origin of this nonphysical noise is analyzed. In the first instance, the applied acoustic far-field analysis method is found to be a limiting factor. A cutoff frequency estimate is obtained beyond which LES prediction is not reliable, but up to which frequency LES prediction was good. Second, the influence of the subgrid-scale model is assessed by the analysis of 1) the effect of reduced deconvolution order and 2) an LES with no subgrid-scale modeling but with spatial filtering after each timestep instead. Additionally, a higher resolution LES is performed with similar filter width as in the original LES to reduce numerical errors close to the filter cutoff. Both reduced deconvolution order and spatial filtering result in a more rapid dropoff of the acoustic far-field spectra up to the cutoff frequency, which is attributed to the higher dissipation in the flow simulation. This suggests that the type of employed subgrid-scale model is not of importance for aeroacoustic prediction, given that enough dissipation is provided to dampen spurious waves, but that as little as possible is provided to reproduce the fluid spectra at higher frequencies.

Nomenclature

c_∞ = ambient speed of sound
E = total energy
G, G_2 = filter transfer function
L_2, L_3 = jet nozzle dimensions
M (M_c) = Mach number (convective)
N = deconvolution order
n_2, n_3 = parameters of the inflow velocity profile
p = pressure
Q_N = deconvolution operator
q_i = heat flux components
R, R_i = direction vector magnitude, components
$\Re$, $\Im$ = real, imaginary part
Re = Reynolds number
T = temperature
$T_{i,j}$ = Lighthill source tensor
t = time
$\boldsymbol{u}$ = vector of conservative variables
$\boldsymbol{x}, \boldsymbol{y}$; x_i, y_i = vector of coordinates; components
Δt = computational time step
Δt_s = sampling interval
δ, δ_i = vorticity thickness, in coordinate direction x_i
η, ζ = cross-stream coordinates normalized by nozzle half-width $L_i/2$, $i = 2, 3$
θ = radiation angle
κ = wave number
κ_c = filter cutoff
λ = wavelength
μ = dynamic viscosity
ρ = density
τ_{ij} = components of the viscous stress tensor
χ, χ_i = relaxation coefficient, components
ω = circular frequency
$*$ = convolution operator

Subscripts

j = jet center quantity
rms = root mean square value
∞ = ambient quantity

Superscripts

d = dimensional quantity
$-$ = filtered quantity
$\star$ = deconvolved quantity
$\check{}$ = computed with filtered quantities
$\check{}\star$ = computed with deconvolved quantities
$*$ = complex conjugate quantity
$'$ = fluctuating quantity

Introduction

LARGE-EDDY simulation (LES) has been well established as a simulation tool to predict turbulent flows at higher Reynolds numbers where direct computation is not feasible. A wide range of models that have been tested and validated with respect to correct flow prediction is currently in use to mimic the effect of scales not represented in an LES. However, when this established LES capability is extended to aeroacoustic problems, additional questions must be addressed concerning the effects of subgrid-scale modeling and numerical errors on the predicted radiated sound.

LES should, in general, be able to reproduce the lower frequencies of the far-field sound originating from resolved fluid scales. The use of low-dissipation subgrid-scale models and high-order nondissipative schemes (like dispersion-relation-preserving[1] and compact[2] schemes) to solve the compressible Navier–Stokes equations can lead to the generation of spurious pressure waves (grid-to-grid oscillations) in a simulation. Even though they are found in many simulations (for example, see Refs. 3 and 4), their treatment is rarely documented. Also, the enforcement of boundary conditions can be a source of unwanted spurious waves.[5] For the computation of statistical mean data, these spurious waves are not of significant importance

---

Presented as Paper 2003-3281 at the AIAA/CEAS 9th Aeroacoustics Conference, Hilton Head, SC, 12–14 May 2003; received 5 June 2003; revision received 26 February 2004; accepted for publication 17 March 2004. Copyright © 2004 by B. Rembold and L. Kleiser. Published by the American Institute of Aeronautics and Astronautics, Inc., with permission. Copies of this paper may be made for personal or internal use, on condition that the copier pay the $10.00 per-copy fee to the Copyright Clearance Center, Inc., 222 Rosewood Drive, Danvers, MA 01923; include the code 0001-1452/04 $10.00 in correspondence with the CCC.

[*] Research Assistant, Institute of Fluid Dynamics. Member AIAA.

[†] Professor, Institute of Fluid Dynamics.

because they are smoothed out by the averaging procedure and have very small amplitudes. However, for acoustic analysis, they cannot be neglected and care has to be taken to suppress their generation and/or to remove them in the simulation or in the data postprocessing. This is particularly important if acoustic and flowfields are to be computed on the same domain. A spectrum of methods is currently being used to ensure enough dissipation in LES simulations for aeroacoustic prediction. Examples are 1) constant eddy-viscosity-type subgrid-scale models, for example, see Ref. 6; 2) the same models as 1 but with the additional use of artificial selective damping[7] at high wave numbers, for example, see Ref. 3; and 3) no use of any subgrid-scale model and additionally neglect of the viscous terms in connection with MILES schemes (see Ref. 8).

In previous work[9] the ability of LES to use the approximate deconvolution model (ADM) for predicting the far-field sound radiation was examined in a comparison of direct numerical simulation (DNS) and LES data of rectangular jet flow. The noise computation employed Lighthill's acoustic analogy in frequency space to compute far-field acoustic spectra from the LES flowfields. It was found that far-field computations based on the filtered LES quantities can reproduce the lower frequency part of the spectrum well. However, spurious noise spoiled the acoustic spectra in the high-frequency domain and led to an overprediction of the overall sound pressure level, particularly in the upstream direction.

In the present study, an attempt is made to analyze the origin of the spurious noise of the LES-based prediction. The far-field sound is analyzed based on Lighthill's acoustic analogy. The role of the deconvolution is examined, and the origin of the spurious waves in the LES is located. Assessments are made based on comparison of far-field spectra and instantaneous dilatation contours of LES and DNS-based data.

The motivation for the choice of a rectangular jet as test case is twofold. On the one hand, nonaxisymmetric nozzle shapes achieve superior mixing with very little loss of thrust compared to a round jet. The basic mechanism relies on the introduction of streamwise vorticity that is responsible for faster mixing and higher entrainment. (See Ref. 10 for a detailed review.) From an acoustic point of view, this enhanced mixing leads to a reduced overall acoustic power output, especially for supersonic jets. On the other hand, the nonaxisymmetry introduces a directivity in the acoustic radiation pattern of the jet that has been confirmed in many experimental studies. (See, for example, Refs. 11 and 12.) Along the minor axis of the jet (the loud plane) a consistently higher acoustic power is observed. The two main reasons for this directivity are acoustic shielding from the (nonaxisymmetric) mean flow around the core of the jet and the different vortex structure behind the nozzle compared to round jets. Whereas round jets tend to break up through helical modes, dominant flapping modes are found in rectangular jets. It can only be speculated which particular vortex topology produces which radiation pattern. Numerical simulations can help to obtain more insight into such phenomena, which makes LES an attractive tool.

Flow Description

The flow test case under investigation was a transitional Mach 0.5 jet issuing from a rectangular nozzle with a Reynolds number of 5×10^3. Nondimensionalization was based on jet center quantities $u_{1,j}$, ρ_j, T_j, and one-half of the longer dimension of the nozzle $L_2/2$. The coordinate system and dimensions are shown in Fig. 1. The temperature ratio of the ambient to jet-center temperature was $T_\infty/T_j = 0.936143$. LES data were compared to DNS data for which the computational domain was $[0, 15] \times [-7, 7] \times [-7, 7]$, and the grid consisted of $337 \times 229 \times 229$ points.[13,14] The corresponding LES simulations were computed on the domain $[0, 18.75] \times [-7, 7] \times [-7, 7]$ by the use of a grid of $141 \times 77 \times 77$ points. For the present case, the LES typically consumed about 2% of CPU time of the DNS when computing the same physical time span.

Inflow and Boundary Conditions

It is generally agreed on that the downstream development of a jet strongly depends on the initial conditions at the jet nozzle. Early work in that field was done by Bradshaw[15] who examined the sensitivity of a mixing layer. Recent publications[16–18] are in agreement with that finding. Ho and Huerre[19] give a review of perturbed shear layers. A very illustrative example about the influence of jet forcing is given in Ref. 20, where the aspect of bifurcation, that is, the separation of the initial jet into two jets caused by strong inflow forcing is summarized.

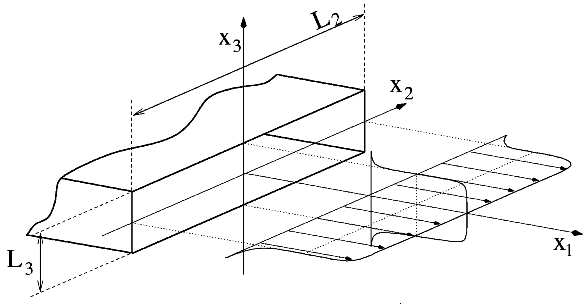

Fig. 1 Jet nozzle geometry and coordinate system.

Parameters that influence the downstream behavior of a jet are the initial shear layer thickness, the shear layer thickness distribution (which strongly depends on the upstream curvature of the nozzle), the nozzle shape, Mach and Reynolds numbers, and the turbulence intensities at the inflow. Additionally, the presence of peaks in the excitation spectrum at the inflow is of more importance than simply the integral turbulent intensity[21] because the mere presence of one frequency can trigger instabilities in the jet if the frequency matches that of an unstable jet mode.

Almost invariably, the collectivity of these parameters is not available from a particular experiment, the reason being that they are not documented or simply partially unknown. This makes it difficult to compare experimental data taken in different facilities and also computational data with experimental data. Inflow conditions of numerical computations can at best be matched to some degree, and it is left to the creativity of the researcher how well an experiment is reproduced by a computation. However, some level of uncertainty remains.

For the present simulations, clearly defined inflow disturbances were enforced to avoid instabilities in the jet that are merely triggered by numerical roundoff errors. We chose an analytical profile on top of which a linear instability mode was superimposed. The artificial inflow profile was chosen according to Yu and Monkewitz[22]:

$$u(\eta, \zeta) = [1 + \sinh[|\eta| \sinh^{-1}(1)]^{2n_2}]^{-1}$$
$$[1 + \sinh[|\zeta| \sinh^{-1}(1)]^{2n_3}]^{-1} \qquad (1)$$

The parameters $n_2 = 9$ and $n_3 = n_2 L_3/L_2$ ensured equal vorticity thicknesses $\delta = \delta_i = L_i/[\sqrt{2}n_i \sinh^{-1}(1)]$ in both directions. The cross-stream velocity components of the laminar inflow profile were set to zero. Transition was triggered by imposition of the most unstable varicose mode of the inflow profile, which was computed according to linear stability theory under the assumption of a parallel profile along the x_3 direction at $x_2 = 0$. (See Ref. 14 for more details.) The disturbance amplitude measured by the maximum of its streamwise velocity component was 0.0025, and the forcing frequency was 2.71. At the edges of the jet ($|x_2| \approx 1$) the forcing was ramped down to zero.

In the LES, the boundary condition at the inflow plane was enforced by a sponge-layer formulation within a narrow region of 10 gridpoints at the inflow. In this region, the governing equations are modified with a forcing term that drives the solution to a (given) target solution. Details of this formulation can be found in Ref. 23. The target profile for the inflow sponge was chosen to be the laminar inflow profile with the superimposed instability wave with a spatial evolution over the inflow sponge region as predicted by linear stability theory. At the lateral and outflow boundaries, nonreflecting boundary conditions[24] were applied, also in connection with a sponge layer. The target solution at the lateral boundaries was the quiet ambient flow. At the outflow, the target solution was dynamically computed during the simulation by spatial and temporal filtering of the flowfield in the outflow sponge region.[13]

LES Equations

We employed ADM as a subgrid-scale model for the present simulations.[25] The basis of ADM is the use of a primary discrete filter (with kernel G) that is explicitly applied to the Navier–Stokes equations (Fig. 2). The unknown terms in the LES (the subgrid-scale stress tensor) are computed directly from approximately deconvolved quantities $\boldsymbol{u}^\star = Q_N \bar{\boldsymbol{u}} \approx \boldsymbol{u}$ that are constructed from the computed filtered fields $\bar{\boldsymbol{u}}$ with an approximate deconvolution operator Q_N. The flux terms are computed directly with the approximately unfiltered fields $\boldsymbol{u}^\star$ and are subsequently filtered with the discrete filter. The operator Q_N is obtained by series expansion of the inverse of the filter G and truncated at finite N. This leads to a regularized approximate deconvolution operator

$$Q_N = \sum_{i=0}^{N} (I - G)^i \approx G^{-1} \tag{2}$$

where I is the identity operator. In numerical tests, the deconvolution order $N = 5$ was found to be sufficient.[25] For higher N, the statistical flow results did not significantly improve.

To model the transfer of energy to the nonresolved small scales, a relaxation term is added that drains energy from the scales beyond the filter cutoff. It has the form $(I - G_2) * \bar{\boldsymbol{u}}$, where G_2 is a secondary filter of high order. In ADM, the secondary filter is constructed as

$$G_2 = Q_N * G \tag{3}$$

This relaxation term operates only in the high-wave-number band ($\kappa > \kappa_c = 2/3\pi$) (to be interpreted in a local sense[26] because no spatial Fourier transform can be defined in complex geometries), and it serves as an energy sink. The term energy has to be interpreted in a generalized sense: The relaxation term operates on all conservative variables, mass, momentum, and energy. Note that this relaxation term is very similar to the concept of artificial selective damping.[7]

The filtered conservation equations (for mass, momentum, and energy) modeled with ADM are, thus,

$$\frac{\partial \bar{\rho}}{\partial t} + \overline{\frac{\partial (\rho u_j)^\star}{\partial x_j}} = -\chi_1(\bar{\rho} - \overline{\rho^\star}) \tag{4a}$$

$$\frac{\partial \overline{\rho u_i}}{\partial t} + \overline{\frac{\partial}{\partial x_j}\left[\frac{(\rho u_i)^\star (\rho u_j)^\star}{\rho^\star} + \check{p}^\star \delta_{ij} - \check{\tau}_{ij}^\star\right]} = -\chi_2\left[\overline{\rho u_i} - \overline{(\rho u_i)^\star}\right] \tag{4b}$$

$$\frac{\partial \bar{E}}{\partial t} + \overline{\frac{\partial}{\partial x_j}\left[(E^\star + \check{p}^\star)\frac{(\rho u_j)^\star}{\rho^\star} - \check{\tau}_{ij}^\star \frac{(\rho u_i)^\star}{\rho^\star} + \check{q}_j^\star\right]} = -\chi_3[\bar{E} - \overline{E^\star}] \tag{4c}$$

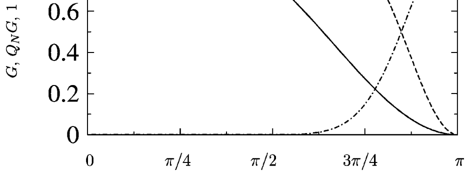

Fig. 2 Transfer functions of the primary filter: ——, G; – – –, Q_NG; and –·–, $1-Q_NG$.

with $i, j = 1, 2, 3$. The star superscript refers to a deconvolved variable and the upside-down caret indicates that the respective quantities are computed according to their definition but with filtered conservative variables. Quantities denoted by both the star and upside-down casat superscript are computed similarly, but with deconvolved variables. [For example, $f(a, b) = ab$, $\check{f} = \bar{a}\,\bar{b}$, and $\check{f}^\star = a^\star b^\star$.] The (spatially and temporally varying) relaxation coefficients χ_i are determined dynamically. More details on the model can be found in Ref. 25. For spatial discretization, a sixth-order (at interior points) compact central scheme[2] is used for all terms. Time integration is performed with a third-order low-storage Runge–Kutta scheme. Detailed code validation against linear stability theory was carried out,[13] and DNS and LES flow results also agreed very well.[23]

Acoustic Analysis

Lighthill's equation[27,28] reads

$$\frac{\partial^2 \rho}{\partial t^2} - c_\infty^2 \frac{\partial^2 \rho}{\partial x_i \partial x_i} = \frac{\partial^2 T_{ij}}{\partial x_i \partial x_j} \tag{5}$$

with the source tensor

$$T_{ij}(\boldsymbol{x}, t) = \rho u_i u_j + \delta_{ij}\left\{p - c_\infty^2 \rho\right\} - \tau_{ij} \tag{6}$$

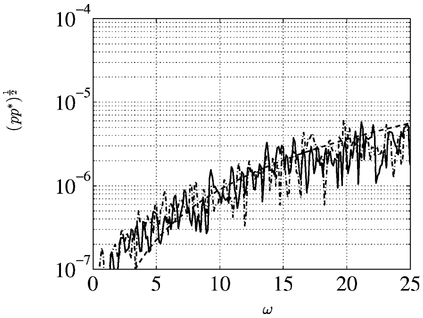

Fig. 3 Far-field spectra for $\theta = 150$ deg, on the arc at radius $60L_2/2$ in the ——, major and –·–, minor jet planes of artificial source field with - - - -, ω^2 increase.

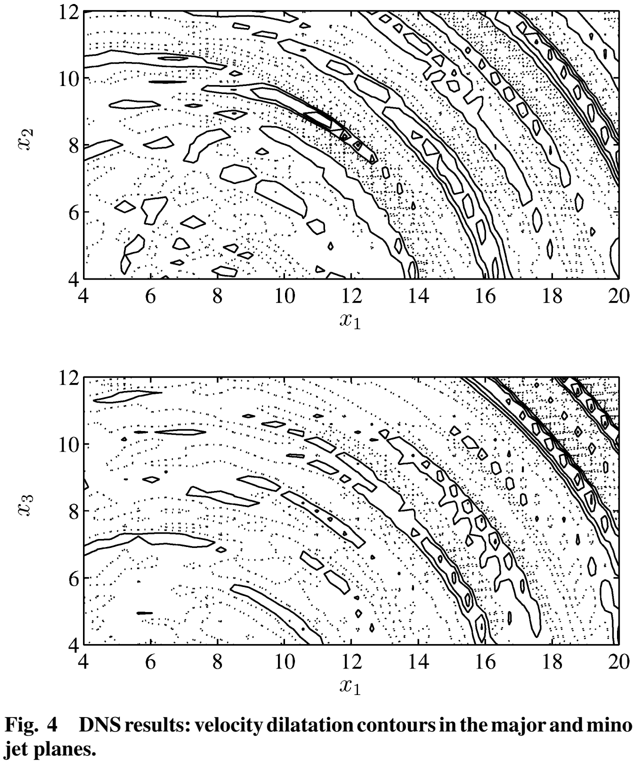

Fig. 4 DNS results: velocity dilatation contours in the major and minor jet planes.

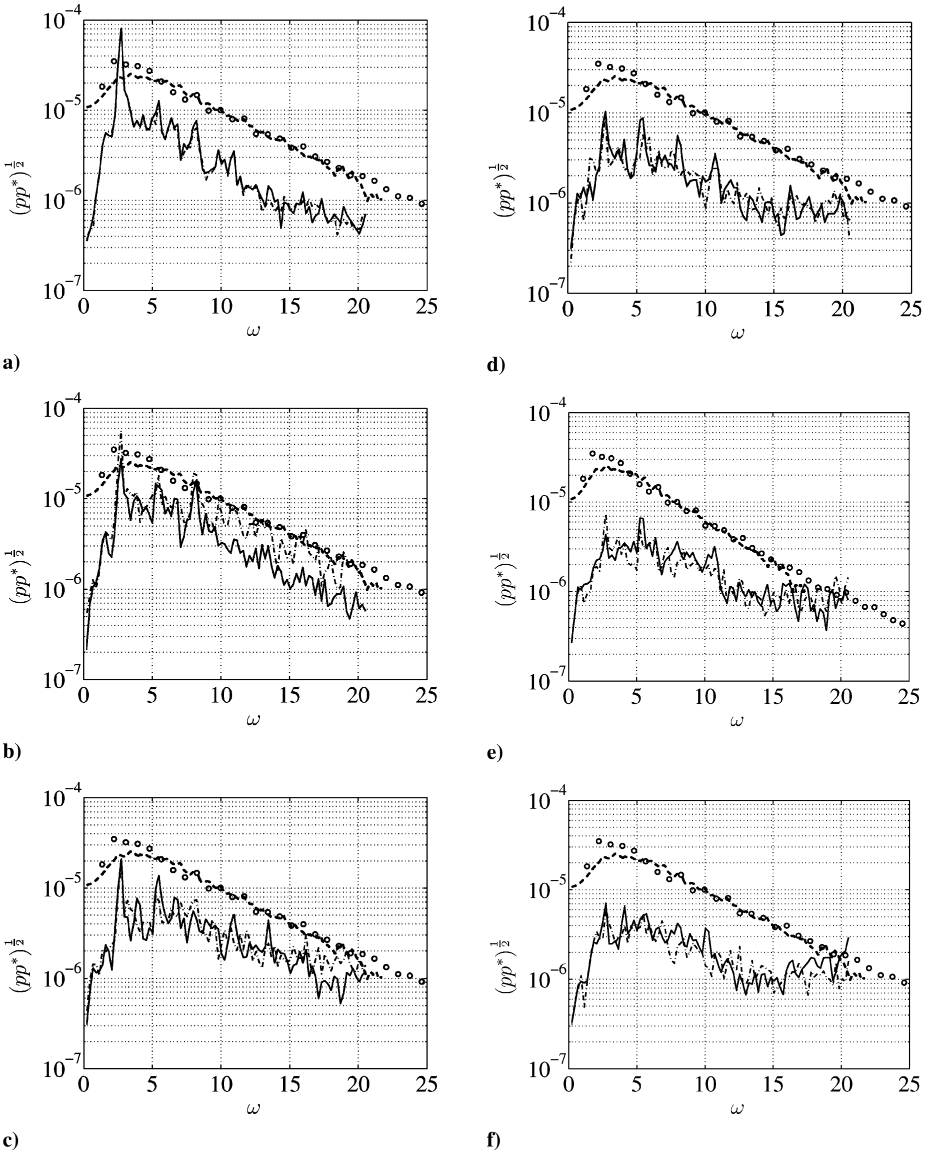

Fig. 5 DNS: far-field spectra for $\theta =$ a) 5, b) 30, c) 60, d) 90, e) 120, and f) 150 deg on the arc at radius $60L_2/2$ in the ——, major and –·–, minor jet planes; also, ○, spectra from a round-jet DNS,[33] and - - -, experiments of Stromberg et al.,[34] at $\theta = 30$ deg.

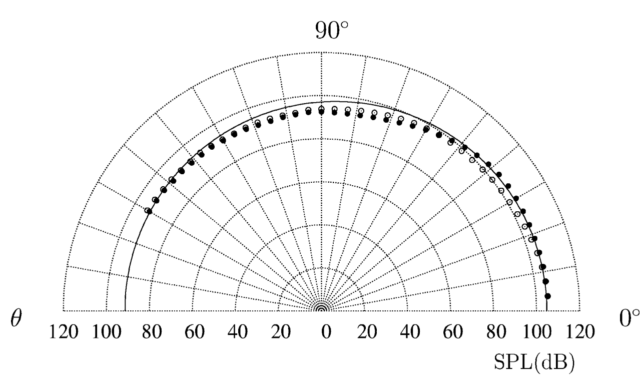

Fig. 6 DNS: SPL along two arcs of radius $60L_2/2$ around the transition area in the ○, major and ●, minor jet planes; ——, expected Doppler scaling.

Here,

$$\tau_{ij} = \mu\left(\frac{\partial u_i}{\partial x_j} + \frac{\partial u_j}{\partial x_i} - \frac{2}{3}\delta_{ij}\frac{\partial u_k}{\partial x_k}\right)$$

is the viscous stress tensor. By the use of $\partial^2 T_{ij}/\partial x_i \partial x_j$ as the equivalent noise source, the far-field sound at point $\boldsymbol{x}$ is evaluated with the free-space Green's function and the divergence theorem as

$$\rho'(\boldsymbol{x}, t) = \rho(\boldsymbol{x}, t) - \rho_\infty = \frac{1}{4\pi c_\infty^4}\int_V \frac{R_i R_j}{R^3}\frac{\partial^2}{\partial t^2} T_{ij}\left(\boldsymbol{y}, t - \frac{R}{c_\infty}\right)\mathrm{d}\boldsymbol{y} \tag{7}$$

where $R = |\boldsymbol{x} - \boldsymbol{y}|$ and $R_i = x_i - y_i$, respectively. Evaluation is simplified by reformulation of Eq. (7) in frequency space, in dimensionless form, as

$$\rho'(\boldsymbol{x}, \omega) = \frac{M_\infty^4}{4\pi}\int_V \frac{R_i R_j}{R^3}\omega^2 T_{ij}(\boldsymbol{y}, \omega) e^{-iM_\infty R\omega}\,\mathrm{d}\boldsymbol{y} \tag{8}$$

which avoids the interpolation needed to compute retarded times in Eq. (7). Both formulations correctly represent the quadrupole nature of the source and have been shown to facilitate an accurate numerical evaluation.[29,30] In evaluating Eq. (8), we neglect τ_{ij} in Eq. (6), which is typically small.[27,31] The second term in the tensor is also small for nearly isentropic flow and, thus, was neglected here as well. It was also recently shown by Freund[32] through analysis of DNS data that those assumptions are valid. Thus, for the present analysis, we retained only $\rho u_i u_j$ in the source tensor (6). Because, for the radiation to the far-field, only the fluctuation of T_{ij} in time is significant [see Eq. (7)], the temporal average can be subtracted. Accordingly, in the following T_{ij} denotes this fluctuation.

A large number of samples in time of the flowfields were used to compute the sound sources. Those sets were subdivided into overlapping subintervals to increase statistical sampling, which is a standard procedure in signal processing. The interval length was chosen to resolve the expected lower frequencies well, in particular, the forcing frequency of the jet. The spectral resolution was given by the temporal resolution of the stored data. The mean-value-corrected Lighthill stress tensor was computed in each interval and time transformed by the use of discrete Fourier transform. The samples were windowed in time with a function constructed from one-half of a period of a cosine function, which ramped the signal smoothly to zero over 50 samples at the beginning and end of each window to avoid spurious high frequencies introduced by the finite sample length. In the DNS, the data were unfortunately stored at slightly nonequidistant intervals, but the change of the interval length was less than 1% and the associated error in the evaluation of Fourier sums was neglected.

Far-field sound spectra were obtained by numerical evaluation of Eq. (8) by the use of a trapezoidal rule quadrature directly on the grid. The source terms T_{ij} tend to zero at large x_2 and x_3 and at the inflow boundary, which allows integration all of the way to the domain boundaries. At the outflow boundary, they are also small compared to their size in the transition area, though not zero because turbulent structures leave the domain. We therefore smoothly ramped down the source terms close to the outflow boundary to avoid affecting the volume integral by leaving sources. It was found that the influence on the particular form of the smoothing function is weak, and, therefore, the same window function as for the Fourier transform in time was applied.

Analysis of Spurious Noise Predicted by LES

In the evaluation of the acoustic emission based on LES data, spurious noise in the high-wave-number region was previously found to spoil acoustic prediction for higher frequencies, especially for upstream radiation angles.[9] When analyzing the origin of this spurious noise, one faces two interwoven phenomena that are difficult to separate. First, the LES flow simulation can actually be polluted by unphysical high-frequency noise, which can be caused, for example, by the LES model. This is discussed hereafter. Second, the acoustic analysis procedure itself has its limits up to which prediction is reliable. Also, the computation of T_{ij} in frequency space can introduce errors due to finite window length, but this influence was found to be negligible. Furthermore, the evaluation of the volume integral (8) in computing the far-field intensities and spectra necessarily introduces errors. During evaluation of DNS results, this is not a problem due to sufficient grid resolution. In the LES it can be a limiting factor.

To remain within the accuracy of the discrete volume integral, the spatial Nyquist frequency must not be exceeded for the integrand. The change of the argument of the exponential term in Eq. (8) must,

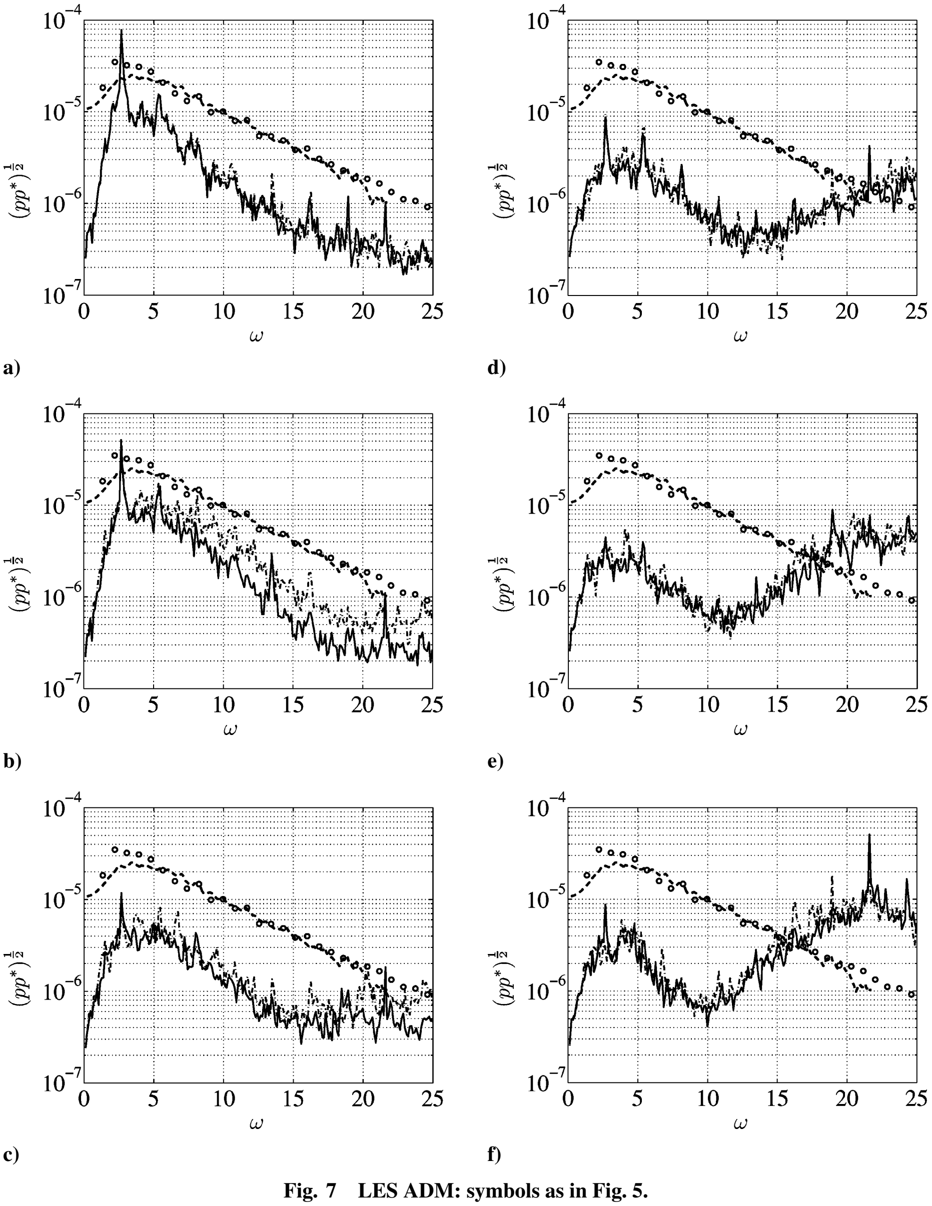

Fig. 7 LES ADM: symbols as in Fig. 5.

therefore, be limited from grid point to grid point as $\pi > M_\infty \omega \Delta R$, which leads to a maximal frequency of $\omega_{\max} \approx 40$, which is not limiting. Under the assumption that the spatial variation of $T_{ij}(\boldsymbol{y}, \omega)$ at a given ω is convection dominated, this variation can be connected to some mean convection velocity u_c. For jets, a good estimate is $u_c = 0.6$, and with a given Nyquist wavelength λ_n given by the grid spacing in the x_1 direction, a maximum temporal frequency of $\omega_{\max} = 2\pi u_c/\lambda_n \approx 14$ can be estimated. Beyond that frequency, the prediction cannot be expected to be accurate and errors amplified by the ω^2 term in Eq. (8) may dominate. This effect can be demonstrated by the use of artificial spatial noise for the T_{ij} fields that is convected with $u_c = 0.6$ in the x_1 direction. This represents a convected frozen turbulence field that, in theory, does not radiate at all. The physically meaningless far-field of such a field with $\Re(T_{ij})$ and $\Im(T_{ij})$ chosen randomly from the interval [0.005:0.005] is shown in Fig. 3. (This corresponds to typical amplitudes for the present jet case at a frequency of $\omega = 12$.) The unphysical increase in the spectra can be clearly observed. For the following analysis, we, therefore, considered only frequencies up to a cutoff frequency of $\omega_c = 12$, up to which numerical integration should be reliable.

The LES results can be themselves affected by high-frequency noise present in the simulation. If the intention is to compute aeroacoustically induced sound directly from an LES flow simulation on the same grid, one has to suppress the generation of any unmeaningful spurious waves in the LES because no spectral separation can be made. To assess the effect of the LES simulation itself on the creation of spurious noise, we investigated the following model variants, which essentially introduce different levels of dissipation at high wave numbers. Additionally, a standard ADM simulation (ADMHI) was performed on a more refined grid, but with the same filter width as the original LES. Thus, we considered the following conditions:

1) M1: The deconvolution in the ADM procedure aims at recovering scales up to the filter cutoff frequency. However, it also amplifies noise in the unphysical high wave number band above the filter cutoff in the LES simulation. A reduced deconvolution order simulation with $N = 2$ was carried out to assess the effect of noise generation by the deconvolution.

2) M2: To eliminate model influences, high-order filtering after every time step without any LES model is applied. Here, sufficient dissipation is ensured solely by filtering all conservative variables using a high-order filter at each time step of the simulation. As a filter, of we used the operator $(G_2)^2 = (Q_N G)^2$.

3) ADMHI: A higher-resolved LES with the unaltered ADM model was performed, albeit with the same physical filter width as in the original LES simulation. The grid was refined here to 183 × 101 × 101. Spurious noise of the order of the Nyquist wave number should be less dominant and also the volume integration more accurate.

In Table 1, the number of samples used for the present analysis are listed for the various cases.

We begin presenting acoustic results from DNS. In Fig. 4, the dilatation of the velocity field

$$\frac{\partial u_i}{\partial x_i} = -\frac{\rho_j}{\rho_\infty}\frac{\partial \rho}{\partial t} \tag{9}$$

is shown in the major and minor axis plane of the jet. It was computed on a 40 × 35 equidistant grid within the plotting range by retransformation of $\rho'(x, \omega)$ from Eq. (8) to physical space. The base wavelength caused by the forcing frequency of the jet can be clearly seen. For Fig. 4, the signals look noisy because only one sample of the DNS time series was used to compute the spectra $T_{ij}(\boldsymbol{x}, \omega)$. In Fig. 5 the far-field spectra $(pp^*)^{\frac{1}{2}}$ along two arcs of radius 60 in the major and minor jet plane are plotted for various radiation angles θ measured from the jet axis. The spectra are highly peaked at the forcing frequency, which is characteristic for such a low-Reynolds-number subsonic transitional jet. As a comparison, we also plot in Fig. 5 the far-field spectrum (arbitrary level) of the

Table 1 Parameters of the acoustic analysis for the various cases, number of samples per subinterval

Case	No. of subintervals	No. of samples	Δt_s
DNS	5	192	0.14
ADM	10	600	0.09
M1	1	600	0.09
M2	1	600	0.09
ADMHI	1	800	0.07

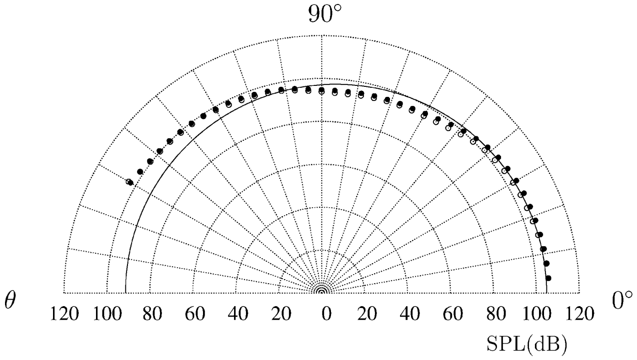

Fig. 8 LES ADM: symbols as in Fig. 6.

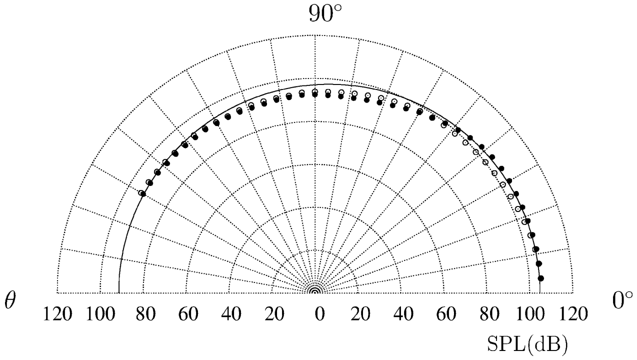

Fig. 9 LES ADM for frequencies up to ω_c, symbols as in Fig. 6.

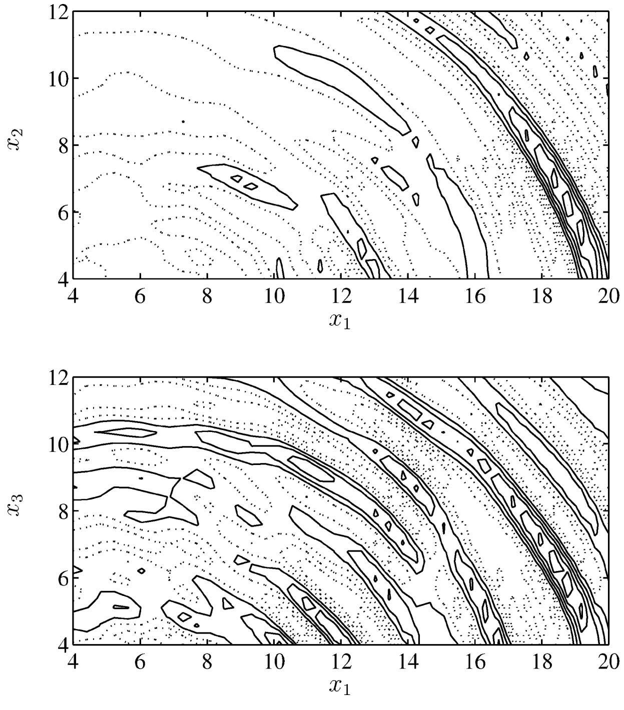

Fig. 10 LES ADM results (frequencies up to ω_c): velocity dilatation contours in the major and minor jet planes.

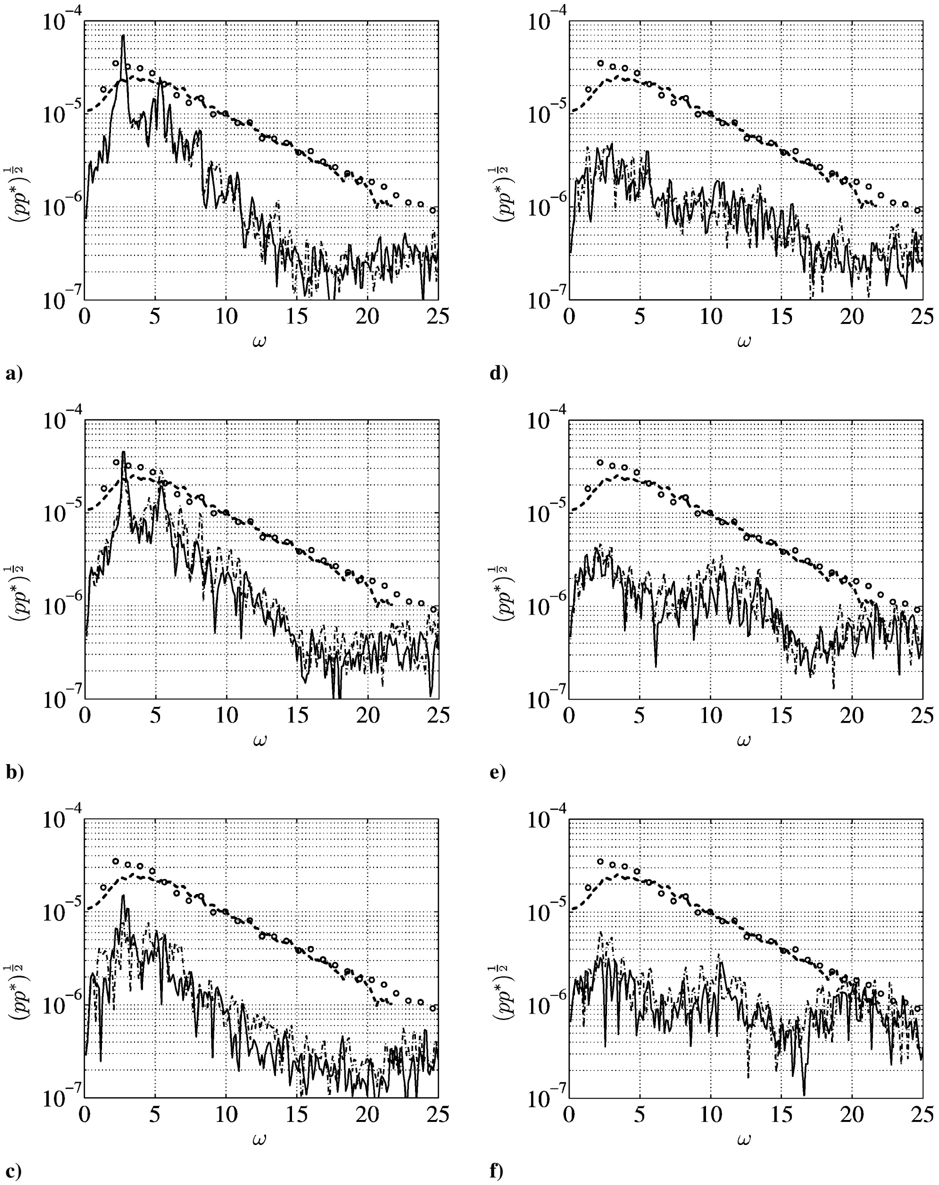

Fig. 11 LES M1: symbols as in Fig. 5.

round jet DNS data of Freund[33] for all angles and experiments of Stromberg et al.[34] at an angle of 30 deg. If the Strouhal number is scaled such that L_3 corresponds to the jet diameter, the dropoff in the spectra is a good match. Experimental observations[12] of a more intense radiation along its minor axis (the loud plane of the jet) are also found in the data.

In Fig. 6, the radiated sound pressure level (SPL) = $20\log_{10}(p^d_{\text{rms}}/p^d_{\text{ref}})$, is plotted for the two arcs, by the use of the standard dimensional reference condition $p^d_{\text{ref}} = 2 \times 10^{-5}$ Pa and under the assumption of standard atmospheric pressure for the computation of the speed of sound. The anticipated directivity based on a Doppler scaling[35]

$$\text{SPL} \sim 1/[1 - M_c \cos(\theta)]^5 \tag{10}$$

with assumed convective Mach number $M_c = 0.6M$ is also plotted. The overall directivity matches very well.

The LES noise prediction based on the original ADM formulation could reproduce the lower frequencies of the acoustic far field; however, the higher frequencies were polluted by spurious noise (Fig. 7). This resulted in an overprediction of the far-field SPL, particularly in the upstream direction of the jet (Fig. 8) The overall prediction was very much improved when the SPL was computed from frequencies up to ω_c (Fig. 9). Accordingly, the far-field dilatation levels for frequencies up to ω_c of the LES (Fig. 10) compare well with the ones from DNS. (Note that the phase angle of excitation is different.) They simply lack the higher wave numbers. This agreement is because the dominant noise sources are at resolved low frequencies.

The reduced deconvolution order simulation (M1), as well as the simulation with high-order filtering (M2) consistently showed a too-rapid dropoff in the spectra (Figs. 11 and 12). This is particularly true for the M2 case. Note that the spectra are much noisier due to little statistical sampling, which, however, does not alter the conclusions. Both simulations catch the transition of the jet reasonably well and correctly predict the low frequencies, especially at the forcing frequency. However, beginning around $\omega \approx 10$, the spectral dropoff compared to the original LES and DNS is too rapid. The M2 simulation is definitely free of spurious noise in the high wave number region; however, the same increase in the spectra at upstream angles can be seen as in Fig. 7. This confirms that the acoustic analysis procedure lacks accuracy in this frequency region. Evaluation of the acoustic far-field based on the ADMHI data showed essentially the same far-field prediction as the original lower resolution LES; however, the spectra reproduced the correct dropoff up to a higher cutoff frequency according to the more refined grid.

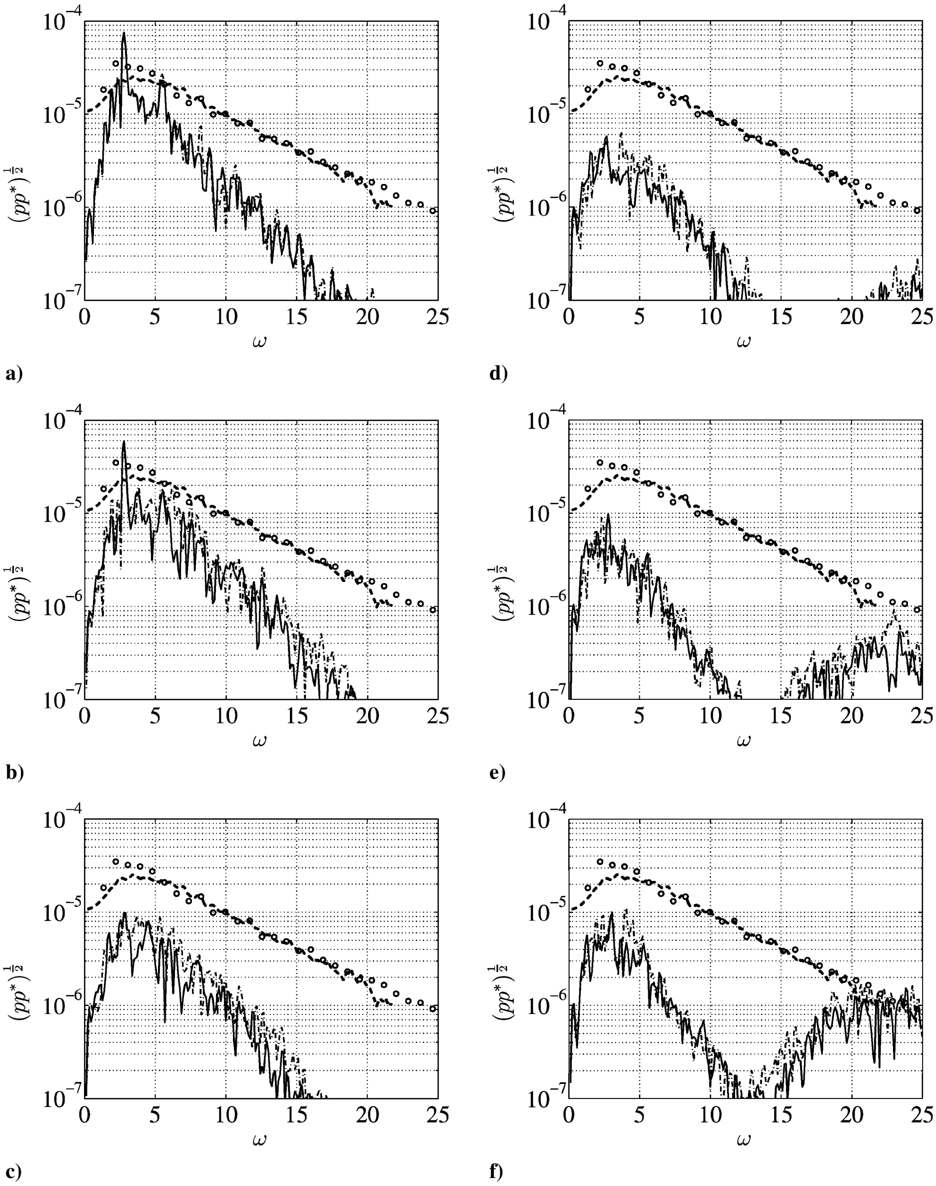

Fig. 12 LES M2: symbols as in Fig. 5.

Conclusions

An analysis of previously found spurious noise in the acoustic radiation prediction of rectangular jet flow from LES data based on Lighthill's analogy was presented. The unphysical increase in the far-field spectra at high frequencies, which resulted in an overprediction of the SPL can be attributed mainly to numerical accuracy limitations of the acoustic analysis procedure. Up to an estimated cutoff frequency, the LES-based prediction is accurate.

To assess the creation of spurious noise by the subgrid-scale modeling in the LES itself, a reduced-order deconvolution simulation ($N = 2$) was performed, as well as an LES with no subgrid-scale modeling that uses high-order filtering only to ensure sufficient dissipation. It was found that both simulations consistently resulted in a too-rapid dropoff of the far-field spectra and that the unphysical increase in the far-field spectra at higher frequencies was nevertheless present. This confirms that this spurious noise was mainly introduced by the acoustic analysis procedure.

The numerical tests suggest that, for aeroacoustic prediction of jet noise by LES, the exact form of the subgrid-scale modeling is not of importance, given that enough dissipation is ensured to dampen spurious noise (grid to grid oscillations) and given that the LES model does not introduce an exceeding amount of dissipation.

Acknowledgments

Funding by the Swiss National Science Foundation is gratefully acknowledged. Computations were performed at the Swiss National Supercomputing Center in Manno, Switzerland. The authors thank J. Freund and M. Wang for their intensive support and very helpful discussions in an earlier stage of this work during the CTR summer program 2002.

References

[1] Tam, C. K. W., amd Webb, J. C., "Dispersion-Relation-Preserving Finite Difference Schemes for Computational Acoustics," *Journal of Computational Physics*, Vol. 107, 1993, pp. 262–281.

[2] Lele, S. K., "Compact Finite Difference Schemes with Spectral-Like Resolution," *Journal of Computational Physics*, Vol. 103, 1992, pp. 16–42.

[3] Bogey, C., Bailly, C., and Juvé, D., "Noise Investigation of a High Subsonic Moderate Reynolds Number Jet Using a Compressible LES," *Theoretical and Computational Fluid Dynamics*, Vol. 16, 2003, pp. 273–297.

[4] Bodony, D. J., and Lele, S. K., "Large Eddy Simulation of Turbulent Jets and Progress Towards a Subgrid Scale Noise Model," *Proceedings LES for Acoustics*, edited by T. Hüttl, C. Wagner, and J. Delfs, German Aerospace Center, DLR, Göttingen, Germany, 2002.

[5] Colonius, T., "Modeling Artificial Boundary Conditions for Compressible Flow," *Annual Review of Fluid Mechanics*, Vol. 36, 2004, pp. 315–345.

[6] Andersson, N., Eriksson, L.-E., and Davidson, L., "Large-Eddy Simulation of a Mach 0.75 Jet," *Proceedings of the 9th AIAA/CEAS Aeroacoustics Conference and Exhibit*, AIAA, Reston, VA, 2003.

[7] Tam, K. W., "Computational Aeroacoustics: Issues and Methods," *AIAA Journal*, Vol. 33, No. 10, 1995, pp. 1788–1796.

[8] Seror, C., Simulation des Grandes Échelles pour la Prédiction du Bruit des Écoulements Turbulents, Ph.D. Dissertation, Université de Paris Sud, U.F.R. Scientifique d'Orsay, Paris, Nov. 2000.

[9] Rembold, B., Freund, J., and Wang, M., "An Evaluation of LES for Jet Noise Prediction," *Proceedings of the Summer Program 2002*, Center for Turbulence Research, Stanford Univ., Stanford, CA, 2002, pp. 5–14.

[10] Gutmark, E. J., and Grinstein, F. F., "Flow Control With Noncircular Jets," *Annual Review of Fluid Mechanics*, Vol. 31, 1999, pp. 239–72.

[11] Kinizie, K. W., and McLaughlin, D. K., "Aeroacoustic Properties of Supersonic Elliptic Jets," *Journal of Fluid Mechanics*, Vol. 395, 1999, pp. 1–28.

[12] Kantola, R. A., "Noise Characteristics of Heated High Velocity Rectangular Jets," *Journal of Sound and Vibration*, Vol. 64, No. 2, 1979, pp. 277–294.

[13] Rembold, B., "Direct and Large-Eddy Simulation of Compressible Rectangular Jet Flow," Ph.D. Dissertation, ETH 15081, ETH Zürich, Zurich, 2003.

[14] Rembold, B., Adams, N. A., and Kleiser, L., "Direct Numerical Simulation of a Transitional Rectangular Jet," *International Journal of Heat and Fluid Flow*, Vol. 23, No. 5, 2002, pp. 547–553.

[15] Bradshaw, P., "The Effect of Initial Conditions on the Development of a Free Shear Layer," *Journal of Fluid Mechanics*, Vol. 26, 1996, pp. 225–236.

[16] Lozanova, M., and Stankov, P., "Experimental Investigation on the Similarity of a 3D Rectangular Turbulent Jet," *Experiments in Fluids*, Vol. 24, 1998, pp. 470–478.

[17] Antonia, R. A., and Zhao, Q., "Effect of Initial Conditions on a Circular Jet," *Experiments in Fluids*, Vol. 31, 2001, pp. 319–323.

[18] Xu, G., and Antonia, R. A., "Effect of Different Initial Conditions on a Turbulent Round Free Jet," *Experiments in Fluids*, Vol. 33, 2002, pp. 677–683.

[19] Ho, C. M., amd Huerre, P., "Perturbed Free Shear Layers," *Annual Review of Fluid Mechanics*, Vol. 16, 1984, pp. 365–424.

[20] Reynolds, W. C., Parekh, D. E., Juvet, P. J. D., and Lee, M. J. D., "Bifurcating and Blooming Jets," *Annual Review of Fluid Mechanics*, Vol. 35, 2003, pp. 295–315.

[21] Hussain, A. K. M. F., "Coherent Structures and Turbulence," *Journal of Fluid Mechanics*, Vol. 173, 1986, pp. 303–356.

[22] Yu, M.-H., and Monkewitz, P. A., "The Effect of Nonuniform Density on the Absolute Instability of Two-Dimensional Inertial Jets and Wakes," *Physics of Fluids A*, Vol. 2, No. 7, 1990, pp. 1175–1181.

[23] Rembold, B., Adams, N. A., and Kleiser, L., "Direct and Large-Eddy Simulation of a Transitional Rectangular Jet," *Direct and Large-Eddy Simulation IV*, edited by B. J. Geurts, R. Friedrich, and O. Métais, Kluwer, Dordrecht, The Netherlands, 2001, pp. 197–204.

[24] Thompson, K. W., "Time Dependent Boundary Conditions for Hyperbolic Systems," *Journal of Computational Physics*, Vol. 68, No. 1, 1987, pp. 1–24.

[25] Stolz, S., Adams, N. A., And Kleiser, L., "The Approximate Deconvolution Model for LES of Compressible Flows and Its Application to Shock-Turbulent-Boundary-Layer Interaction," *Physics of Fluids*, Vol. 13, No. 10, 2001, pp. 2985–3001.

[26] Vasilyev, O. V., Lund, T. S., and Moin, P., "A General Class of Commutative Filters for LES in Complex Geometries," *Journal of Computational Physics*, Vol. 146, 1998, pp. 82–104.

[27] Lighthill, M., "On Sound Generated Aerodynamically, I, General Theory," *Proceedings of the Royal Society of London, Series A: Mathematical and Physical Sciences*, Vol. 211, No. 1107, 1952, pp. 564–587.

[28] Lighthill, M., "On Sound Generated Aerodynamically, II, Turbulence as a Sound Source," *Proceedings of the Royal Society of London, Series A: Mathematical and Physical Sciences*, Vol. 222, No. 1148, 1954, pp. 1–32.

[29] Bastin, F., Lafon, P., and Candel, S., "Computation of Jet Mixing Noise Due to Coherent Structures: The Plane Jet Case," *Journal of Fluid Mechanics*, Vol. 335, 1997, pp. 261–304.

[30] Wang, M., "Computation of Trailing-Edge Noise at Low Mach Number Using LES and Acoustic Analogy," *Annual Research Briefs*, Center for Turbulence Research, Stanford, CA, 1998.

[31] Goldstein, M. E., *Aeroacoustics*, McGraw–Hill, New York, 1976.

[32] Freund, J. B., "Noise-Source Turbulence Statistics and the Noise from a Mach 0.9 Jet," *Physics of Fluids*, Vol. 15, No. 6, 2003, pp. 1788–1799.

[33] Freund, J. B., "Noise Sources in a Low-Reynolds-Number Turbulent Jet at Mach 0.9," *Journal of Fluid Mechanics*, Vol. 438, 2001, pp. 277–305.

[34] Stromberg, J. L., McLaughlin, D. K., and Troutt, T. R., "Flow Field and Aeoustic Properties of a Mach Number 0.9 Jet at a Low Reynolds Number," *Journal of Sound and Vibration*, Vol. 72, No. 2, 1980, pp. 159–176.

[35] Crighton, D. G., "Basic Principles of Aerodynamic Noise Generation," *Progress in Aerospace Sciences*, Vol. 16, No. 1, 1975, pp. 31–96.

P. Givi
Associate Editor